Proceedings of 2013 2nd International Conference on Advances in Electrical Engineering (ICAEE 2013)
19-21 December, 2013, Dhaka, Bangladesh

Design of a Tunable High Q Photonic Band Edge Cavity on Ferroelectric Barium Titanate

Ashfaqul Anwar Siraji*† and M. Shah Alam*†
*Department of Electrical and Electronic Engineering
Northern University Bangladesh
†Department of Electrical and Electronic Engineering
Bangladesh University of Engineering and Technology (BUET)
†Email: shalam@eee.buet.ac.bd

***Abstract*—A band edge cavity on ferroelectric Barium Titanate is proposed. The cavity is designed by inserting a Photonic Crystal (PhC) within another PhC, so that the band edge of the core PhC falls within the band-gap of the outer PhC, which supports the slow light modes of the inner PC. The PhCs are selected based on their band diagram which is calculated by Plane Wave Expansion (PWE) method. The spectral purity, spatial and time confinement of the cavity are then studied using Finite Domain Time Difference (FDTD) method. The frequency spectrum of the designed cavity is calculated from the time response of the cavity. At the resonant wavelengths, the field profile and quality factors (Q) are calculated. The dispersive and absorptive nature of $BaTiO_3$ is included in the calculation. It is found that the proposed cavity can sustain three high Q comparable modes. It has also been found that the tunability of the proposed band edge cavity is weaker compared to that of a photonic band-gap defect cavity.**

***Keywords*—High Q, Band Edge Cavity, Slow Light Mode, Barium Titanate.**

I. Introduction

Photonic crystal (PhC) structures have become extremely efficient in manipulating light in increasingly subtle ways. Photonic crystal cavities offer tight confinement of light in space, time and frequency with amazing versatility [1]–[3]. Photonic crystal slab devices are specially attractive because they provide three dimensional confinement but their operation is very similar to that of two dimensional (2D) photonic devices. 2D photonic crystal cavities based on such slabs has been used in many different devices with many different advantages [4]–[6]. There are two distinct approaches towards designing 2D PhC slab cavities. In one approach, one introduces a defect in the structure. This defect creates a state in the photonic band-gap of the structure and constitutes the cavity [9]. In the other approach, one makes use of slow light modes (SLM) with low group velocity at the edges of the band diagram of a PhC geometry [10], [11]. The chief disadvantage of following the former approach is that any fault in fabricating the defect may alter the properties of the cavity. In the latter approach, the crystal contains no defect. While such cavities are less sensitive to fabrication error, they are spatially delocalized compared to defect cavities.

We analyse a cavity where the SLM at the bandedge of the "core" PhC structure is spatially localized by a surrounding "mirror" PhC structure. In the core PhC structure, the resonant modes have low group velocity. Hence they can be sustained for a long period of time, providing high spectral purity. At the same time, the modes fall within the band-gap of the "mirror" PhC, which localizes the modes spatially. Bordas *et al.* have provided a detailed designing method for such bandedge cavity structure in [10]. In this work, we have followed a similar designing principle keeping ferroelectric $BaTiO_3$ as the base material. As the $BaTiO_3$ is an attractive optical material because it's optical properties can be tuned electrically, several tunable PhC devices have been proposed using $BaTiO_3$ [9], [12], [13], but to the best of our knowledge, a tunable bandedge cavity is yet to be reported.

In this work, a tunable photonic band edge cavity on $BaTiO_3$ is proposed. Using 2D plane wave expansion (PWE) method, we design the cavity so that the core PhC has a air band edge within the band-gap of the mirror structure. Using 2D finite difference time domain (FDTD) method along with the fast fourier transform (FFT), we calculate the frequency spectrum of the cavity. Also, the resonant frequencies, the transverse electric mode profiles and the quality factors of the resonant

modes are calculated. The dependance of the resonant properties on the air hole radius is studied. Furthermore, the possibility of a tunable band edge cavity is explored by studying the effect of very small change in the refractive index of the base material on the resonant wavelengths of the cavity.

II. Cavity Design

The cavity is designed on a 400 nm thick slab of $BaTiO_3$ on a substrate of MgO. The slab is patterned with a triangular array of air holes. The period of the lattice, $a = 1\mu$m and the radius of the air holes $r = 0.39a$. The mode of interest in the structure is the transverse electric (TE) modes. The photonic band diagram for this geometry is shown in Fig. 1(a). The band diagram of a PhC depends on it's nanostructure. Thus, the band-gap of the PhC can be changed by changing the radius of air holes. In Fig. 1(b), the evolution of the position and size of the band-gap with respect to change in the radius of air holes is shown. In the figure, we can see that for $r = 0.39a$ (the blue vertical line), the band-gap is between $\frac{a}{\lambda} = 0.3657$ to $\frac{a}{\lambda} = 0.4753$ (the shaded area). It is evident that a second PhC with the same geometry and $0.39a < r < 0.46a$ would have it's dielectric band maxima (where the group velocity $v_g = \frac{d\omega}{dk}$ is very low) within the band-gap of the first PhC. This is the fundamental concept of the band edge cavity.

To design the band edge cavity, a "core" PhC ($r = 0.45a$) is surrounded by a "mirror" PhC which has smaller air holes ($r = 0.39a$). From Fig. 1(b), it can be seen that the dielectric maxima of the core falls within the band-gap of the mirror PhC. The modes of the "core" PhC at the band edge would have very low v_g while being surrounded by a band-gap mirror. In combination, these effects should produce a highly confined mode.

Following the above principles, we design the cavity as shown in Fig. 2. The cavity consists of 20 concentric hexagons. The 6 hexagons in the center have a radius of $r = 0.45a$ and acts as the core. The outer hexagons have a radius $r = 0.39a$ and act as the mirror. To ease the transition, radius of air holes is gradually decreased to $R = 0.39a$ from $r = 0.45a$ over a transition layer with $r = 0.42a$.

III. Method of Calculation

To find the resonant frequency of the band edge cavity, it is excited with a large range of frequencies.

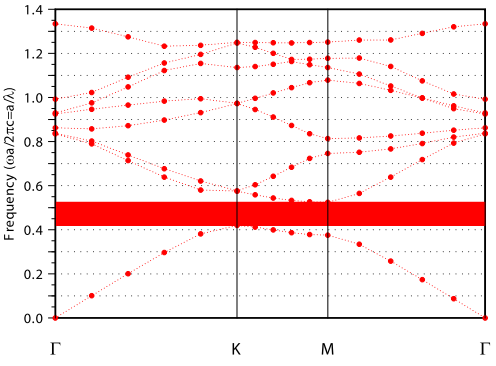

(a)

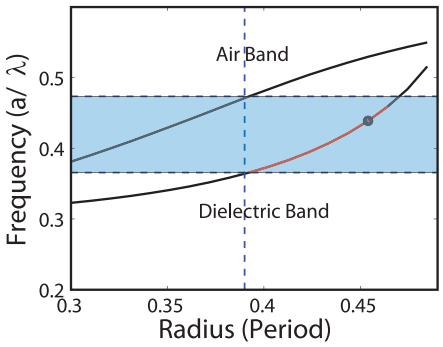

(b)

Fig. 1: (a) The band diagram of the triangular lattice photonic crystal with $r = 0.39a$ for the transverse electric mode. The maxima of the dielectric band is at the K point and the minima of the air band is at the M point. (b) The change in the position and size of the band-gap with respect to change in the radius of the air holes. The radius in plotted in terms of the Period a and the band edges are plotted in normalized frequency.

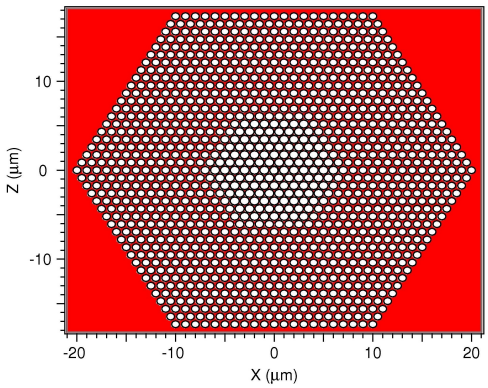

Fig. 2: The structure of the band edge cavity. The central part with larger air holes acts as the core where light is confined. The outer shell with smaller air holes acts as a miiror.

The excitation is allowed to propagate freely in the cavity. Most of the frequencies do not excite the cavity and their energy leaves the cavity quickly. The resonant frequencies excite the cavity and their energy decay very slowly. Hence, the resonant frequencies come as sharp peak in the frequency spectrum. A 2-D FDTD method is used to carry out the calculations. In the two dimensional structure, only the transverse electric modes are of interest.

The initial field is a broadband impulse applied at the core. Only the $\mathbf{H}_y$, $\mathbf{E}_x$ and $\mathbf{E}_z$ components of the TE modes need to be calculated in the time domain. The Yee's mesh is used for discretization of the simulation domain in both space and time, thus reducing the Maxwell's curl equation into simple difference equations. The space grid is setup uniformly so that there are exactly 24 grid points per period, which provides sufficiently converged results. A time step $\Delta t = 5.20833 \times 10^{-17} s$ is used, which is many times smaller than the Courrant limit, but produces sufficient frequency resolution at the expense of simulation time.

In order to solve the Maxwell's equations for this structure, the material properties of the structure must be specified. The dependence of its optical properties on frequency of incident light is calculated from first principle calculations. We obtained the frequency dependence of the complex refractive index ($\tilde{n} = n + i\kappa$), where n is the real part representing the index of refraction and κ is the imaginary part representing the loss component, as shown in Fig. 3. This dispersive and absorptive nature of $BaTiO_3$ is incorporated in the calculations by setting $\epsilon_{i,j} = n_{i,j}^2$ in the FDTD difference equations, where $n_{i,j}$ describes the frequency dependent spatial distribution of the refractive index. At the wavelength of interest, the magnetic properties of the material is negligible. Hence, the relative permeability is set to $\mu_r = 1$.

To excite the structure using an impulse, a suitable initial launch condition is necessary. In this work, the initial excitation $\phi(\mathbf{r}, t)$ consists of the spatial $A(\mathbf{r})$ and temporal $B(t)$ components. The spatial component is a Gaussian field source and the temporal component is a delta impuse function. The excitation is given by,

$$\phi(\mathbf{r}, t) = \exp(\frac{x^2}{a^2}) \exp(\frac{z^2}{a^2}) \delta(t - t_0), \qquad (1)$$

where $a = \frac{Width}{2} = 20\mu m$ and $\delta(t-t_0)$ is a delta impulse function in the time domain. Since the structure is finite, the perfectly matched layer (PML) boundary conditions is used at all sides. This allows the energy incident on the boundary to leave the structure with minimum reflection.

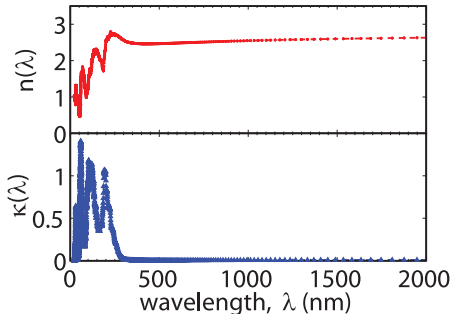

Fig. 3: The refractive index (n) and absorption coefficient(κ) of $BaTiO_3$ against the wavelength. The refractive index is shown on top and the absorption coefficient is on the bottom.

IV. Results and Discussion

A. Frequency Response and Tunability

The structure in Fig. 2 is excited by a broadband impulse specified in (1). Subsequently, the impulse is allowed to propagate freely and it's evolution in the time domain is recorded. While recording time domain data, care was taken to ensure that the data werenot taken from a zero point in the cavity. After the time domain data were recorded, the frequency spectrum is easily calculated by using fast fourier transform (FFT). The resultant spectrum is shown in Fig. 4(a). We can see that the frequency spectrum has sharp peaks at wavelengths $\lambda = 2.4734\mu$m, $\lambda = 2.586\mu$m and 2.709μm. The presence of sharp peaks indicate that the electromagnetic radiation of the mentioned wavelengths stays within the cavity far longer than radiations of other wavelengths, i.e., the mentioned wavelengths are the resonant wavelengths. The studied structure has three resonant TE modes, which are separated by more than 100 nm. The difference between the resonant frequencies indicate that they are not degenerate modes separated by mesh coarseness. The three resonant modes are increasingly further from the dielectric band-edge of the mirror PhC.

The base material of the cavity is ferroelectric $BaTiO_3$, which is an electro-optic material. It's refractive index can be actively tuned using an applied electric field. We have demonstrated the tunability of a PhC cavity on $BaTiO_3$ by performing calculations with a step increase (δn) of 0.01 in the refractive index of the base material in [13]. Using a similar methodology, we calculated the frequency response of the cavity with and

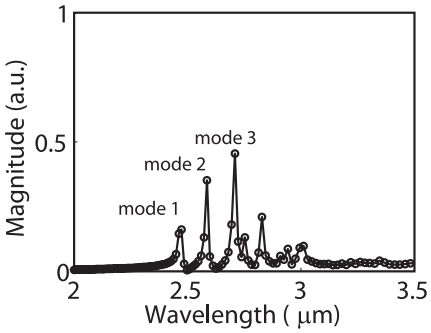

(a)

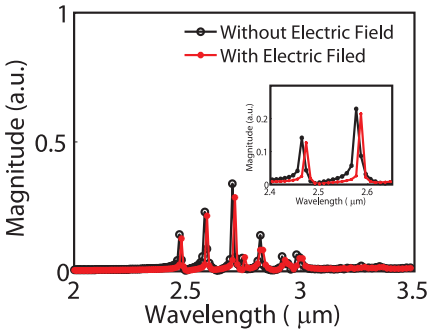

(b)

Fig. 4: (a) Frequency response of the cavity. The strength of the H_y component of the TE mode is plotted against the wavelength. (b) Frequency response of the cavity with and without applied electric field. The first two peaks are shown in the inset to illustrate the tunability of the device.

without applied electric field, as shown in Fig. 4(b). It can be seen that the resonant peaks are slightly moved to higher wavelengths when an electric field in applied. In the inset of the Fig. 4(b), the first two peaks are shown to elucidate this effect. It can be seen that the three resonant modes are moved by 8 nm, 10 nm and 11 nm respectively. Although this change demonstrates dynamic tunability of the device, it is much weaker than previously reported changes in resonant wavelengths [9], [13], [14].

The resonant wavelength of the device is strongly dependent on the air hole radius of the "core" PhC. This is shown in Fig. 5. All three modes show monotonously decreasing resonant wavelength as the "core" air hole radius is increased from $r = 0.40a$ to $r = 0.46a$.

B. Spatial Confinement

Once the resonant frequencies are known, the field profile of the cavity for those frequencies can be calculated. The H_y component of the resonant TE modes

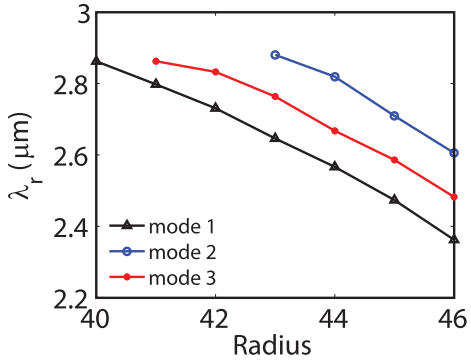

Fig. 5: The impact of "core" air hole radius on the resonant wavelengths of the three modes. The air hole radius is shown as percentage of the PhC period.

are shown in Figs. 6(a), 6(b) and 6(c). The biggest peak remain in the air hole at the centre and then the fields slowly decays away. In the core region, the fields have several smaller peaks. At the boundary between the core and the mirror region, there are several slightly higher peaks. The fields decay very rapidly in the mirror and becomes zero within two periods.

In the Fig. 7, the field strength of the three modes along the X and Z axis respectively are plotted. It can be clearly seen that the fields decay slowly within the core and diminishes to zero within two periods into the mirror. The transition region hastens the decay, but in all cases, a strong peak exists at the onset of the transition area. This due to the sudden change in the band-gap. Through clever manipulation of the air hole placement, this peak can be eliminated.

C. Temporal Confinement

After the field profiles have been calculated, the quality factor (Q) of the cavity can be calculated. The resonant field profile is applied as the initial field and then the field is allowed to propagate freely in time domain. The decaying temporal profile of the total energy density with respect to time is then calculated, where the total energy density is the sum of electric and magnetic field energies given as

$$S(t) = \frac{1}{2}\int_V \left(\epsilon(\mathbf{r})|\mathbf{E}(t)|^2 + \mu|\mathbf{H}(t)|^2\right) dV. \qquad (2)$$

From the temporal profile, the Q factor can be easily calculated. In Fig. 8(a), the temporal profile of the first mode is shown. A similar curve is also calculated for the other modes. The Q factor of the three modes are 4309.7, 4123.5 and 4098.6 respectively. This indicates that all

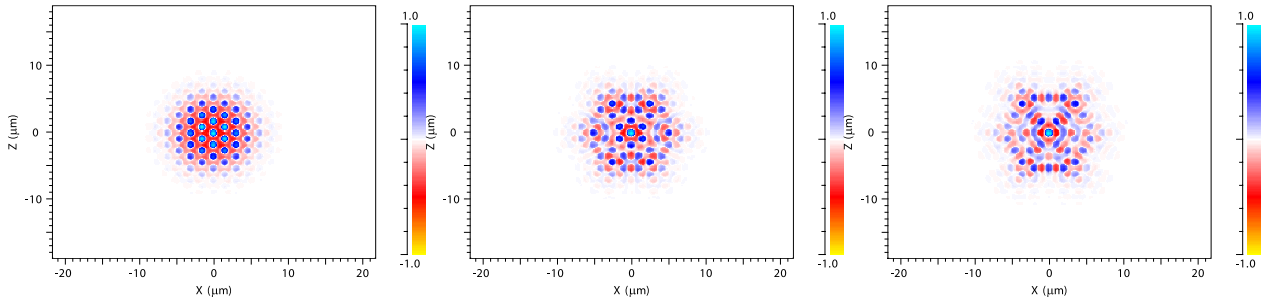

(a) Mode 1 (b) Mode 2 (c) Mode 3

Fig. 6: The H_y field profile at the resonant wavelengths (a) $\lambda_r = 2.473\mu$m, (b) $\lambda_r = 2.586\mu$m, (c) $\lambda_r = 2.709\mu$m

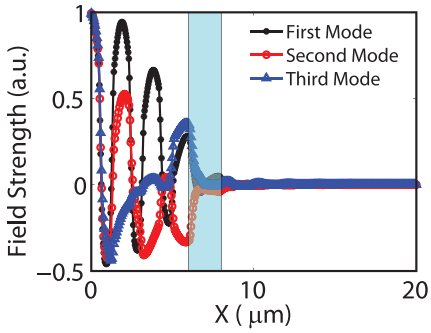

(a)

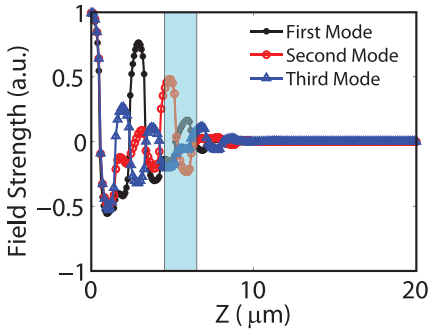

(b)

Fig. 7: (a) The relative strength of the magnetic field (H_y) of the TE modes along the X axis, (b) the relative strength of the magnetic field (H_y) of the TE mode along the Z axis. The shaded area represents the transition between the core and mirror region..

modes are equally suitable for operations requiring high spectral purity. It was noted that the three resonant peaks of the cavity are increasingly further from the dielectric band edge of the "mirror" PhC. Here, it can be seen that the modes near the dielectric band edge of the "core" has the highest Q factor while the modes away from the dielectric band edge has lower Q factors. This indicates

TABLE I: Comparison of quality factor of this work with previous reported values.

Reference	Material	Quality Factor
Makarova *et al.* [7]	Si	396
Kim *et al.* [5]	GaN	550
Giannopoulus *et al.* [8]	InGaAs/InP	2400
This work	$BaTiO_3$	6033

that strong mode mismatch between that "mirror" and "core" PhC results in higher loss and lower Q factor. The result obtained in this work is compared to those available in recent literature in Table I. We have chosen the instances where the setup (i.e., the substrate and base materials, thickness, period etc.) is similar to the one used here. It can be seen that the results presented here compares well with previous literature. The Q of the device is strongly dependent on the air hole radius of the "core" PhC. Bigger air holes pushes the "core" SLM deeper into bandgap of the "mirror", which should enhance the Q factor. This is shown in Fig. 8(b). All three omdes show increasing Q factors as the "core" air hole radius changes.

V. Conclusion

we have designed a band edge photonic crystal cavity on triangular lattice using ferroelectric $BaTiO_3$ and analyzed its confinement capability. The cavity was formed by surrounding a "core" PhC structure with higher air hole radius by a "mirror" PhC structure with smaller air hole radius. The air band edge of the core PhC falls within the bandgap of the mirror PhC. Thus the slow mode at the critical points of the air band of the core is confined by the bandgap of the mirror, producing high spectral purity, quality factor and spatial localization. It

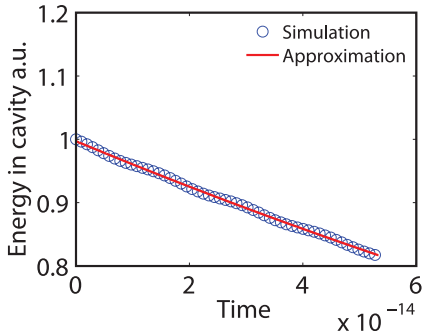

(a)

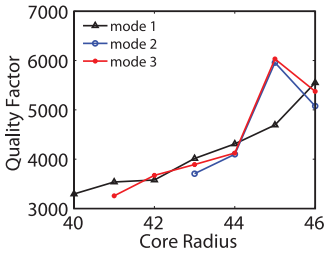

(b)

Fig. 8: (a) The decaying temporal profile of the total energy in the cavity. The decay can be approximated as a decaying exponential. Q factor can be calculated from the decay constant of the approximated exponential (b) The impact of "core" air hole radius on the Q factors of the three modes. The air hole radius is shown as percentage of the PhC period.

was shown that the structure has three resonant TE mode. The quality factor and resonant mode field profile for the TE modes were calculated. It was deduced that the modes with less mismatch has higher Q. The impact of air hole radius of the "core" PhC is studied. It was found that the Q factor rises with increasing air hole radius while the resonant wavelengths monotonically decrease. Although the base material is absorptive, the calculated Q factors are of the same order as the Q factors reported for similar structures in the literature. The designed cavity has a large range of application in optical communication by virtue of it's high quality factor and ability to sustain multiple frequencies simultaneously.

REFERENCES

[1] T. Inoue, M. De Zoysa, T. Asano, and S. Noda, "Single-peak narrow-bandwidth mid-infrared thermal emitters based on quantum wells and photonic crystals," *App. Phys. Lett.*, vol. 102, no. 19, pp. 191 110–191 110–4, 2013.

[2] R. Bchir, A. Bardaoui, and H. Ezzaouia, "Design of silicon-based two-dimensional photonic integrated circuits: Xor gate," *IET Optoelectron.*, vol. 7, no. 1, pp. 25–29, 2013.

[3] H. Fujii, Y. Wang, K. Watanabe, M. Sugiyama, and Y. Nakano, "High-aspect ratio structures for efficient light absorption and carrier transport in ingaas/gaasp multiple quantum-well solar cells," *IEEE J. Photovolt.*, vol. 3, no. 2, pp. 859–867, 2013.

[4] Y. Zhang, M. Khan, Y. Huang, J. Ryou, P. Deotare, R. Dupuis, and M. LonCar, "Photonic crystal nanobeam lasers," *App. Phys. Lett.*, vol. 97, no. 5, p. 051104, 2010.

[5] D.-U. Kim, S. Kim, J. Lee, S.-R. Jeon, and H. Jeon, "Free-standing gan-based photonic crystal band-edge laser," *IEEE Photon. Technol. Lett.*, vol. 23, no. 20, pp. 1454 –1456, Oct. 2011.

[6] R. Shankar, R. Leijssen, I. Bulu, and M. Lončar, "Mid-infrared photonic crystal cavities in silicon," *Opt. Express*, vol. 19, no. 6, pp. 5579–5586, Mar. 2011.

[7] M. Makarova, Y. Gong, S.-L. Cheng, Y. Nishi, S. Yerci, R. Li, L. Negro, and J. Vuckovic, "Photonic crystal and plasmonic silicon-based light sources," *IEEE J. Sel. Topics Quantum Electron*, vol. 16, no. 1, pp. 132 –140, Jan. 2010.

[8] A. V. Giannopoulos, Y.-J. Li, C. M. Long, J.-M. Jin, and K. D. Choquette, "Optical properties of photonic crystal heterostructure cavity lasers," *Opt. Express*, vol. 17, no. 7, pp. 5379–5390, Mar. 2009.

[9] A. A. Siraji, M. S. Alam, and S. Haque, "Impact of space modulation on confinement of light in a novel photonic crystal cavity on ferroelectric Barium Titanate," *J. Lightw. Technol.*, vol. 31, no. 5, pp. 802 –808, Mar. 2013.

[10] F. Bordas, M. J. Steel, C. Seassal, and A. Rahmani, "Confinement of band-edge modes in a photonic crystal slab," *Opt. Express*, vol. 15, no. 17, pp. 10 890–10 902, Aug. 2007.

[11] K. Srinivasan and O. Painter, "Fourier space design of high-q cavities in standard and compressed hexagonal lattice photonic crystals," *Opt. Express*, vol. 11, no. 6, pp. 579–593, Mar. 2003.

[12] M. J. Dicken, L. A. Sweatlock, D. Pacifici, H. J. Lezec, K. Bhattacharya, and H. A. Atwater, "Electrooptic modulation in thin film barium titanate plasmonic interferometers," *Nano Lett.*, vol. 8, no. 11, pp. 4048–4052, 2008.

[13] A. A. Siraji and M. S. Alam, "A tunable photonic double heterostructure cavity on ferroelectric barium titanate," *IEEE Photon. Technol. Lett.*, vol. 25, no. 17, pp. 1676–1679, 2013.

[14] X. Chew, G. Zhou, F. S. Chau, and J. Deng, "Nanomechanically tunable photonic crystal resonators utilizing triple-beam coupled nanocavities," *IEEE Photon. Technol. Lett.*, vol. 23, no. 18, pp. 1310 –1312, Sept. 2011.